ESI file for

Chemisorption of SO_2 and NO_2 gas over $Na_{0.4}MnO_2$ in ambient conditions: An experimental and theoretical study

Nishesh Kumar Gupta[a,b,†*], Kaptan Rajput[c,d,†], Srungarpu N. Achary[e], Rushikesh P. Dhavale[f], Bijal R. Mehta[d], Debesh R. Roy[d], Kwang Soo Kim[a,b**]

Experimental

Chemicals

Sodium acetate trihydrate ($CH_3COONa·3H_2O$), manganese(II) acetate tetrahydrate ($Mn(CH_3COO)_2·4H_2O$) were procured from Sigma Aldrich, Germany. Commercially available SO_2 (100 ppm) and NO_2 (100 ppm) diluted in air were used in the present work.

Analytical instruments

The field emission scanning electron microscopy (FE-SEM, Hitachi S-4300, Hitachi, Japan) was employed to investigate the surface morphology. X-ray diffraction patterns were obtained on an Ultima IV (Rigaku, Japan) X-ray diffractometer with Cu Kα radiation (λ = 1.5406 Å) and a Ni filter in the range of 2θ = 5-100°. The specific surface area and porosity of the samples were analysed by assessing the standard N_2 adsorption-desorption isotherm at −196 °C using a Gemini 2360 series (Micromeritics, United States) instrument, after degassing at 200 °C for 6 h. The chemical states of the elements in the prepared samples were determined by X-ray photoelectron spectroscopy (XPS: Nexsa X-Ray Photoelectron Spectrometer System, Thermo Scientific, United Kingdom), using a monochromatic Al Kα X-ray source, and the spectra were charge-corrected to the main line of the C 1s spectrum (aromatic carbon) set to 284.7 eV. The CasaXPS software (version 2.3.14) was used to analyse the spectra, using GL(p) = Gaussian/Lorentzian product formula, where the mixing is determined by m = p/100. GL(100) is a pure Lorentzian, while GL(0) is a pure Gaussian. In this study, GL(30) was used.

Breakthrough studies

A Pyrex tube was packed with 0.2 g of the oxide between glass wool, and column measurements were performed at 25 °C by passing 100 ppm of SO_2 or NO_2 gas (diluted in air) at a flow rate of 0.2 L min^{-1}. To examine the effect of moisture, the samples were fully saturated with moisture by blowing moist air (80% relative humidity) at 25 °C before passing the gas. The effluent gas was analysed for SO_2 concentration using a GASTIGER 6000 SO_2 analyser, while the NO_2 and NO concentrations in the effluent gas were simultaneously analysed using a GASTIGER 6000 NO_x analyser. The experiments were terminated at the

breakthrough point, defined as the point where the outlet gas concentration reached 20 ppm in this study. The adsorption capacity (q, mg g^{-1}) at the breakthrough point was determined using the following equation:

$$q = \frac{C_0 Q}{m} \int_0^{t_b} \left(1 - \frac{C}{C_0}\right) dt \quad (1)$$

C_0 – initial gas concentration, Q – gas flow rate, m – the mass of oxide, and t_b – breakthrough time.

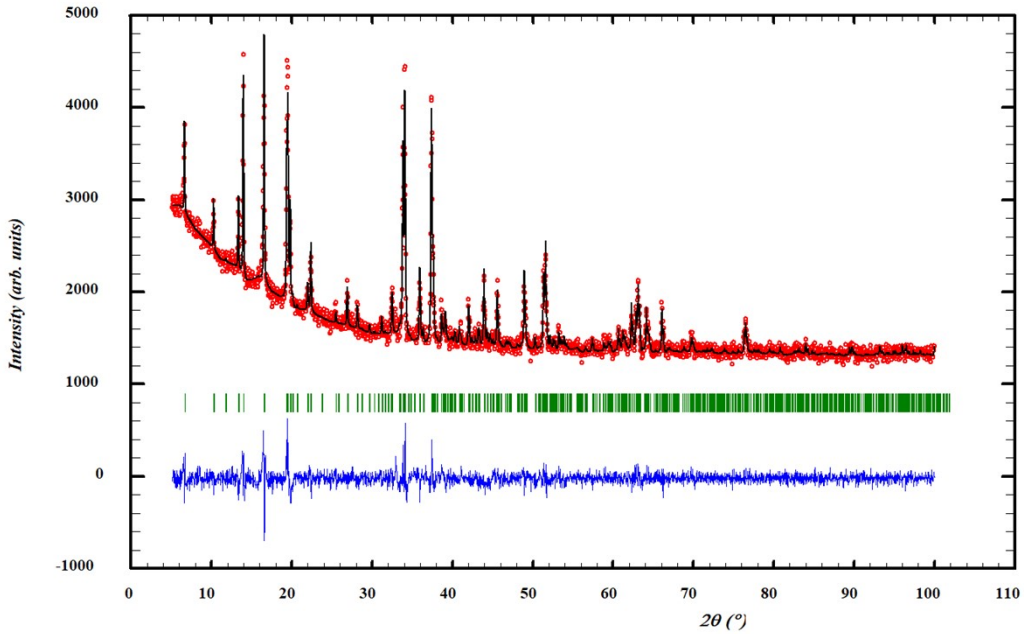

Figure S1. Rietveld refinement plot of $Na_{0.4}MnO_2$. The recorded pattern is shown with black dots, and the calculated pattern and its residual are shown with solid blue and red lines, respectively. Vertical ticks indicate the positions of the Bragg peaks for different phases. R_p: 2.52%, R_{wp}: 3.37%, χ^2: 1.88, R_B: 12.1%, R_F: 13.7 %.

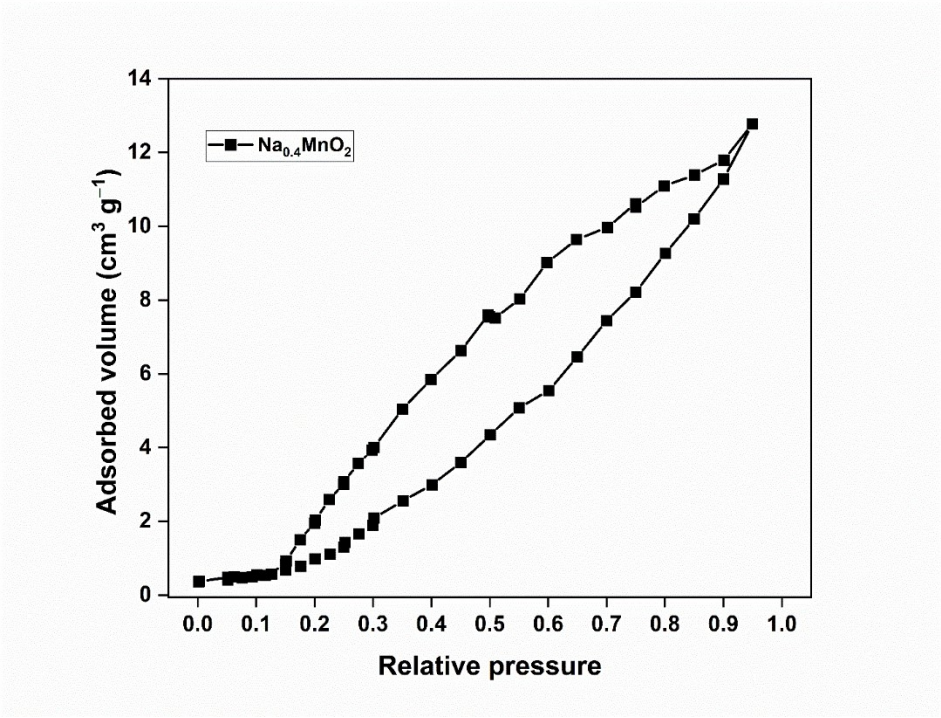

Figure S2. N_2 adsorption-desorption isotherm of $Na_{0.4}MnO_2$.

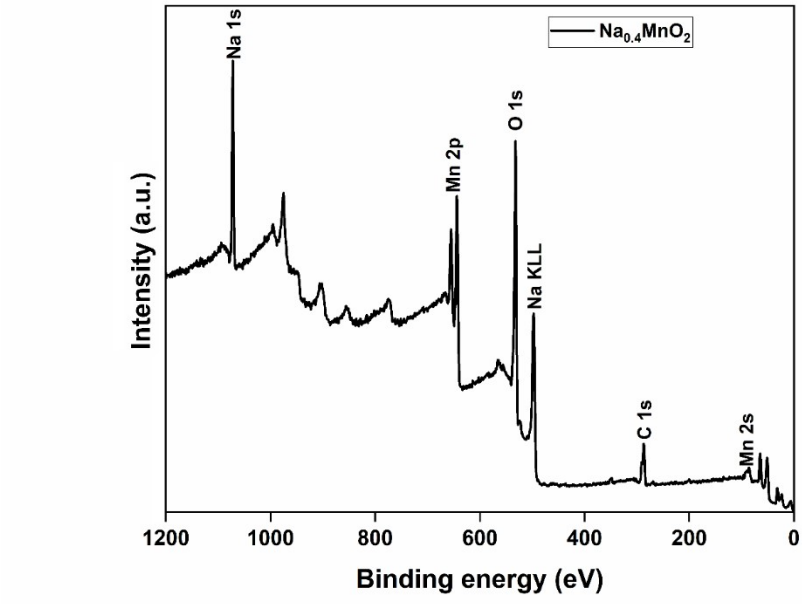

Figure S3. XPS survey of $Na_{0.4}MnO_2$.

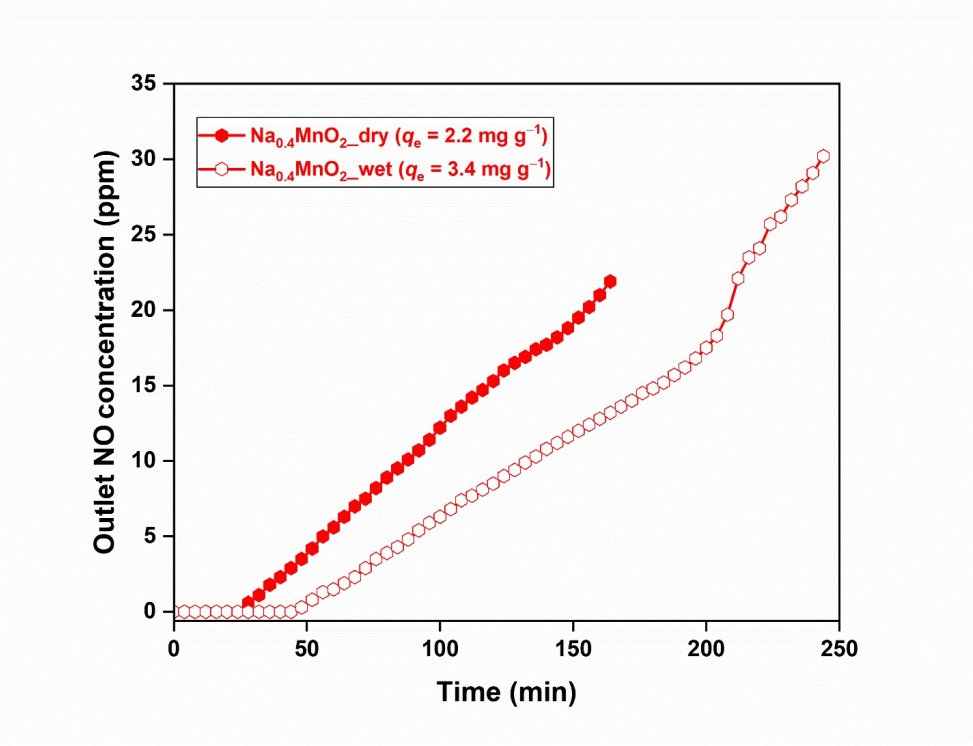

Figure S4. The outlet NO concentration during the NO_2 breakthrough study.

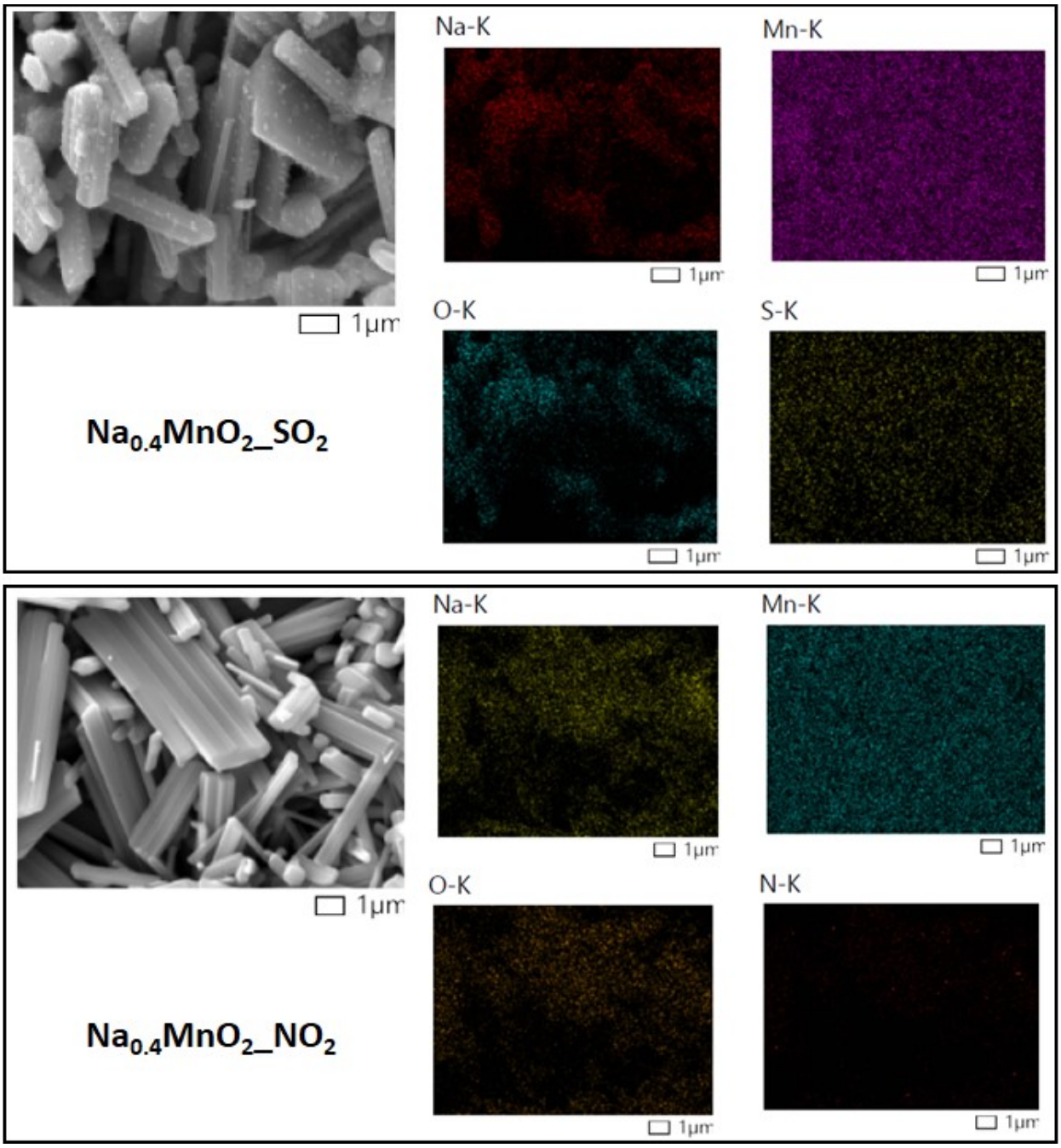

Figure S5. 2D elemental mapping of gas-exposed $Na_{0.4}MnO_2$.

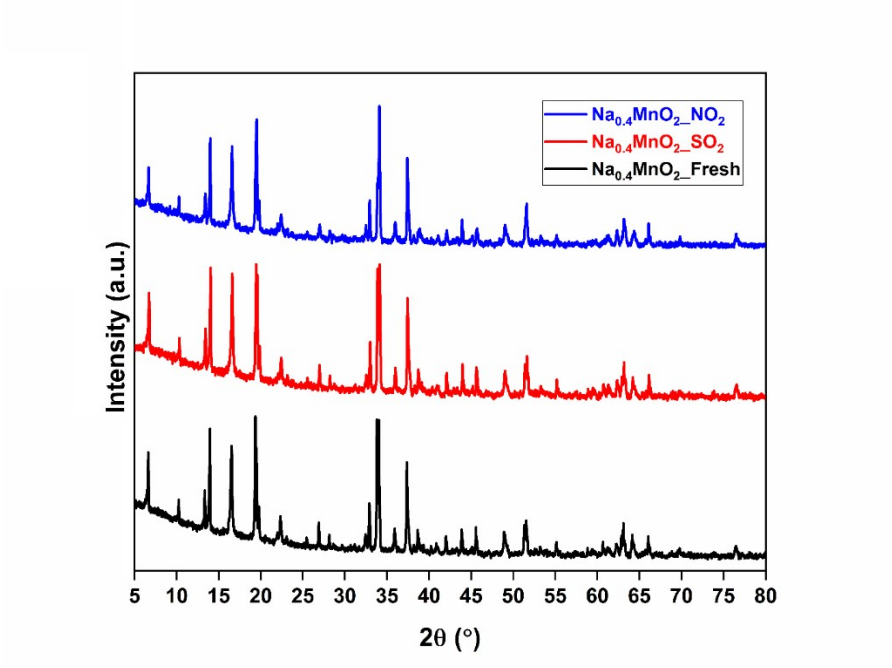

Figure S6. PXRD patterns of fresh and gas adsorbed $Na_{0.4}MnO_2$.

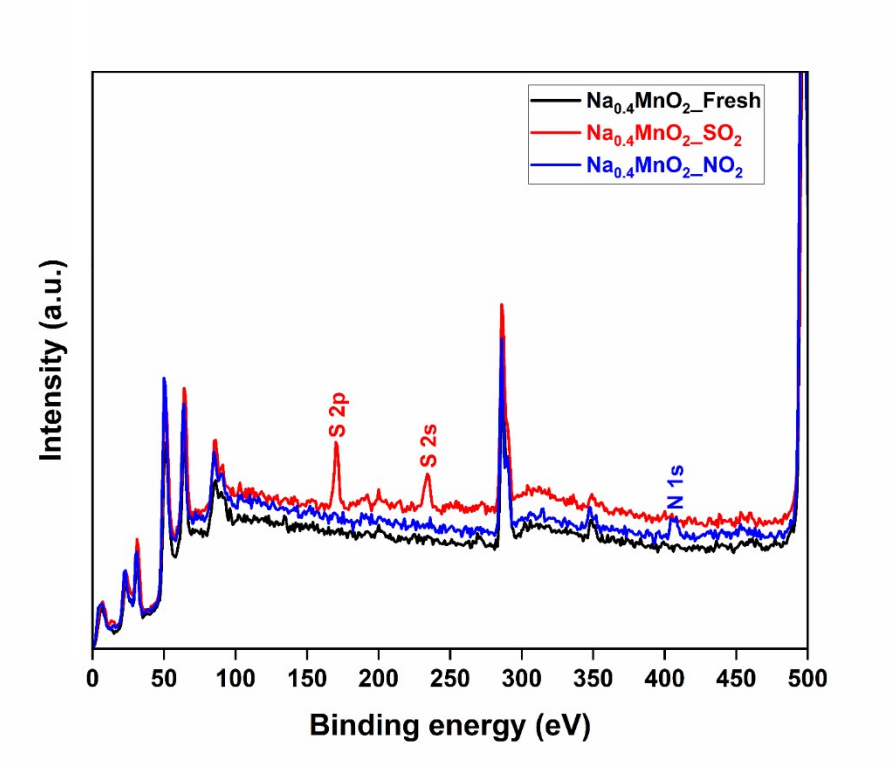

Figure S7. XPS surveys (0-500 eV) of fresh and gas adsorbed $Na_{0.4}MnO_2$.

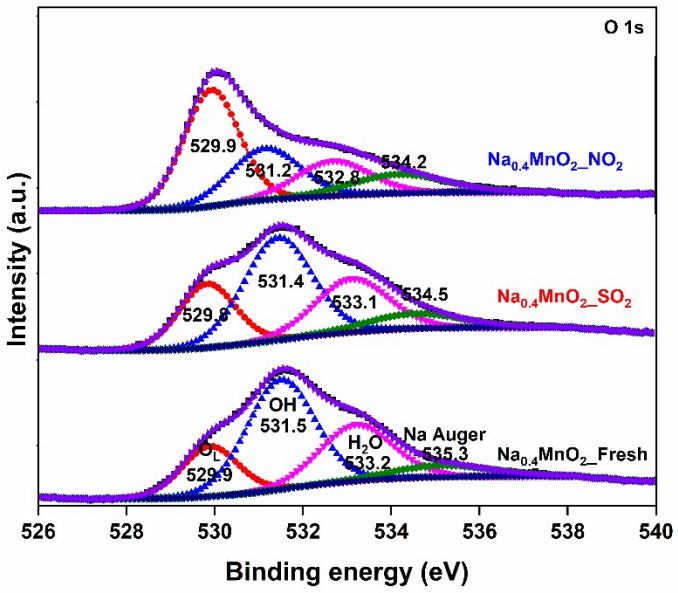

Figure S8. XPS O 1s spectra of fresh and gas-exposed $Na_{0.4}MnO_2$.

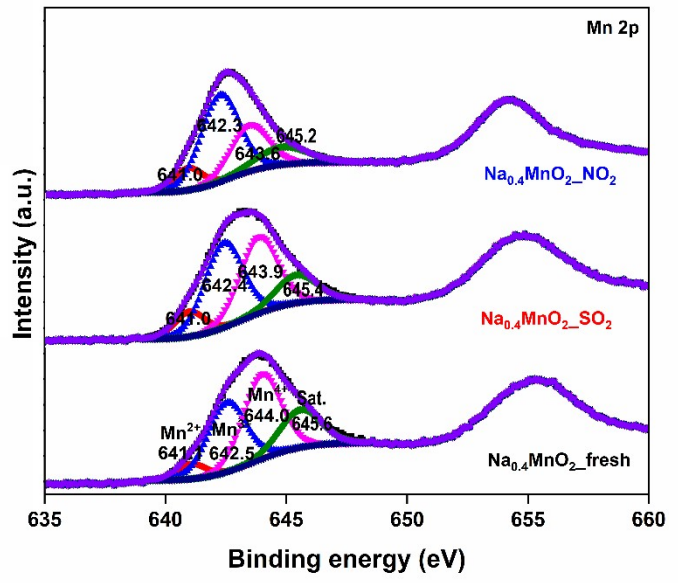

Figure S9. XPS Mn 2p spectra of fresh and gas-exposed $Na_{0.4}MnO_2$.

Table S1. The peak fitting results of the high-resolution Mn $2p_{3/2}$ signal of fresh and gas-exposed $Na_{0.4}MnO_2$ samples.

Sample	Assignment	E_B (eV)	FWHM (eV)	At. %
$Na_{0.4}MnO_2$_Fresh	Mn^{2+}	641.1	1.4	6.7
	Mn^{3+}	642.5	1.8	42.0
	Mn^{4+}	644.0	1.9	51.3
	Satellite	645.6	2.0	-
$Na_{0.4}MnO_2$_NO_2	Mn^{2+}	641.0	1.4	10.9
	Mn^{3+}	642.3	1.8	58.1
	Mn^{4+}	643.6	1.9	31.0
	Satellite	645.2	2.5	-
$Na_{0.4}MnO_2$_SO_2	Mn^{2+}	641.0	1.4	10.8
	Mn^{3+}	642.4	1.8	46.8
	Mn^{4+}	643.9	1.9	42.4
	Satellite	645.4	2.0	-

Table S2. The peak fitting results of the high-resolution O 1s signal of fresh and gas-exposed $Na_{0.4}MnO_2$ samples.

Sample	Assignment	E_B (eV)	FWHM (eV)	At. %
$Na_{0.4}MnO_2$_Fresh	O−Na, O−Mn	529.9	1.5	19.7
	OH	531.5	1.8	51.5
	Water	533.2	1.9	28.8
	Na Auger	535.3	2.6	-
$Na_{0.4}MnO_2$_NO_2	O−Na, O−Mn	529.9	1.5	51.3
	OH	531.2	1.8	28.3
	Water	532.8	1.9	20.4
	Na Auger	534.2	2.5	-
$Na_{0.4}MnO_2$_SO_2	O−Na, O−Mn	529.8	1.5	24.8
	OH/S−O	531.4	1.8	48.1
	Water	533.1	1.9	27.1
	Na Auger	534.5	2.5	-

Table S3. The peak fitting results of the high-resolution N 1s/S 2p signal of fresh and gas-exposed $Na_{0.4}MnO_2$ samples.

Sample	Assignment	E_B (eV)	FWHM (eV)	At. %
$Na_{0.4}MnO_2$_NO_2	Nitrite	404.1	2.0	43.7
	Nitrate	407.1	2.4	56.3
$Na_{0.4}MnO_2$_SO_2	Sulphate	168.4	1.6	38.3
	Bisulphate	170.1	2.0	61.7

Computational details

A theoretical exploration employing Density Functional Theory (DFT) was undertaken to scrutinize the characteristics of the pristine $Na_{0.4}MnO_2$ surface, and the adsorption behaviour of NO_2 and SO_2 gas molecules on the $Na_{0.4}MnO_2$ surface. Computational simulations were conducted using the Vienna Ab initio Simulation Package (VASP), which integrates the projector augmented wave (PAW) method and the generalized gradient approximation (GGA) technique. This combined methodology ensures a precise and comprehensive treatment of ion-electron interactions [1-5]. To elucidate the structural and electronic attributes, a cutoff energy of 500 eV was employed, and Brillouin zone integration was carried out using a Monkhorst-Pack scheme [6] with a k-point grid of 5 × 5 × 1. Throughout the geometric relaxation process, stringent convergence criteria were applied to the total energy and atomic forces, with thresholds set at 10^{-4} eV and 0.02 eV/Å, respectively. For precise assessment of gas molecule adsorption on the surface, van der Waals interactions were rigorously considered and explicitly incorporated into the calculations using the DFT-D3 method [7]. A 15 Å vacuum region was introduced to mitigate spurious imaginary surface interactions. Structural representations of the system were generated using the VESTA package [8]. The adsorption energy (E_{ad}) of the NO_2/SO_2 gas molecule onto the $Na_{0.4}MnO_2$ surface was computed through,

$$E_{ad} = E_{Na_{0.4}MnO_2 + NO_2/SO_2} - E_{Na_{0.4}MnO_2} - E_{NO_2/SO_2} \quad (1)$$

In the equation, the first three components on the right-hand side represent the ground state energy of the $Na_{0.4}MnO_2$ surface, the energy corresponding to the isolated NO_2/SO_2 gas molecule, and the energy associated with the complex configuration of the examined NO_2/SO_2 gas molecules, respectively. The classification of the gas molecule as a donor or acceptor was determined through Bader charge analysis [9]. The charge density difference ($\Delta\rho$) is defined as follows:

$$\Delta\rho = \rho_{Na_{0.4}MnO_2 + NO_2/SO_2} - \rho_{NO_2/SO_2} - \rho_{Na_{0.4}MnO_2} \quad (2)$$

Within the equation, the initial, second, and third terms on the right-hand side signify the charge density of the composite system, the charge density of the gas molecule in isolation, and the charge density of the

$Na_{0.4}MnO_2$ surface, respectively. The Hubbard correction terms for d-states of Mn, as proposed by Dudarev and co-workers [10], have been adopted, along with the GGA functional. In our calculation, U = 4 eV [11] has been adopted as suggested by Shishkin *et al*. The (001) surface has been identified as the most prominent for maximizing the available surface for adsorption activity. It is noteworthy that, in the context of gas molecule adsorption on the surface, the influence is primarily confined to the first few layers. Thus, whether the surface is dense or not is of lesser significance. The dominant adsorption activity is determined by the specific adsorption site and lattice behaviours.

Results and discussions

To investigate potential adsorption interactions involving NO_2 and SO_2 gas molecules with the $Na_{0.4}MnO_2$ surface, the (001) plane of the bulk $Na_{0.4}MnO_2$ within its orthorhombic structural lattice was considered. The top and side views of the bulk orthorhombic phase of $Na_{0.4}MnO_2$ are presented in **Fig. S10(a)**. Additionally, **Fig. S10(b)** displays the (001) plane of bulk $Na_{0.4}MnO_2$ in both top and side views. The well-optimized lattice parameters for the bulk $Na_{0.4}MnO_2$ material within the orthorhombic unit cell are a = 9.125Å, b = 25.321 Å, and c = 2.757 Å. To facilitate the adsorption of gas molecules on the (001) $Na_{0.4}MnO_2$ surface, a supercell was constructed with dimensions of 1 × 1 × 2. The configurations of these supercell structures are depicted in **Fig. S10(b)**.

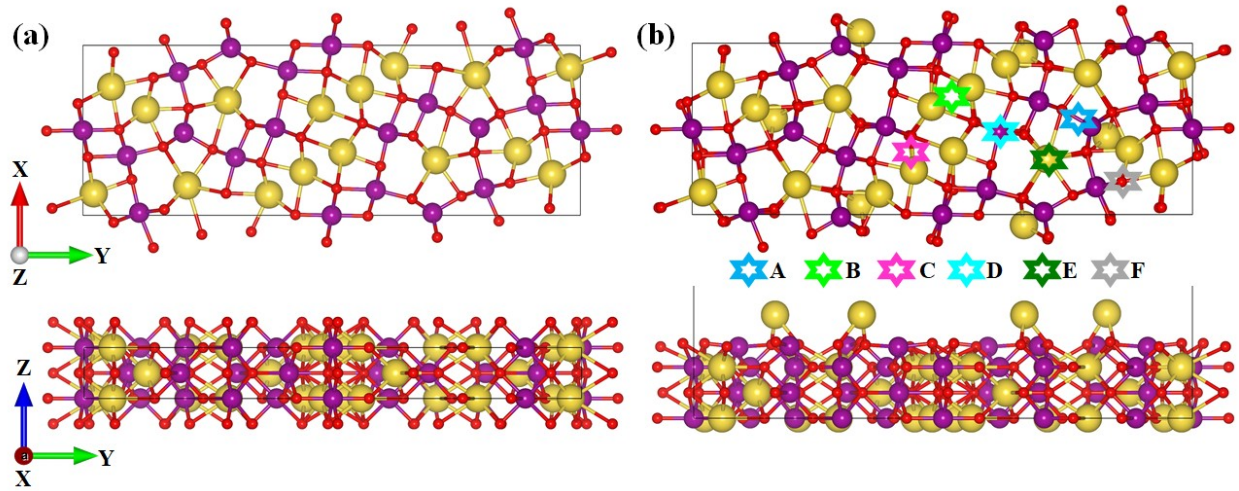

Figure S10. (**a**) The top and side views of the optimized bulk $Na_{0.4}MnO_2$ material within an orthorhombic lattice. The (001) surface of the orthorhombic $Na_{0.4}MnO_2$ material is specifically chosen for investigating its potential for gas molecule adsorption, as illustrated in (**b**). In the top figure of (**b**), various potential adsorption site configurations are denoted by star symbols and labelled from **A** to **F**. The colour codes used are as follows: Na (Yellow), Mn (Violet), and O (Red)

To examine the gas adsorption behaviour of NO_2 and SO_2 molecules on the $Na_{0.4}MnO_2$ surface, six potential adsorption sites labelled as **A** (Mn−O bond), **B** (Na−Na bond), **C** (Na−O bond), **D** (On Mn), **E** (On Na), and **F** (On O) were investigated. These designations corresponded to specific atomic positions on the $Na_{0.4}MnO_2$ surface, as indicated in **Fig. S10(b)**. Subsequently, NO_2 and SO_2 gas molecules were introduced to these specified sites, positioned approximately 3 Å above the $Na_{0.4}MnO_2$ surface. Following a successful relaxation process, optimized geometries for NO_2 and SO_2 gas molecules at each designated site were obtained, as illustrated in **Fig. S11** and **S12**, respectively.

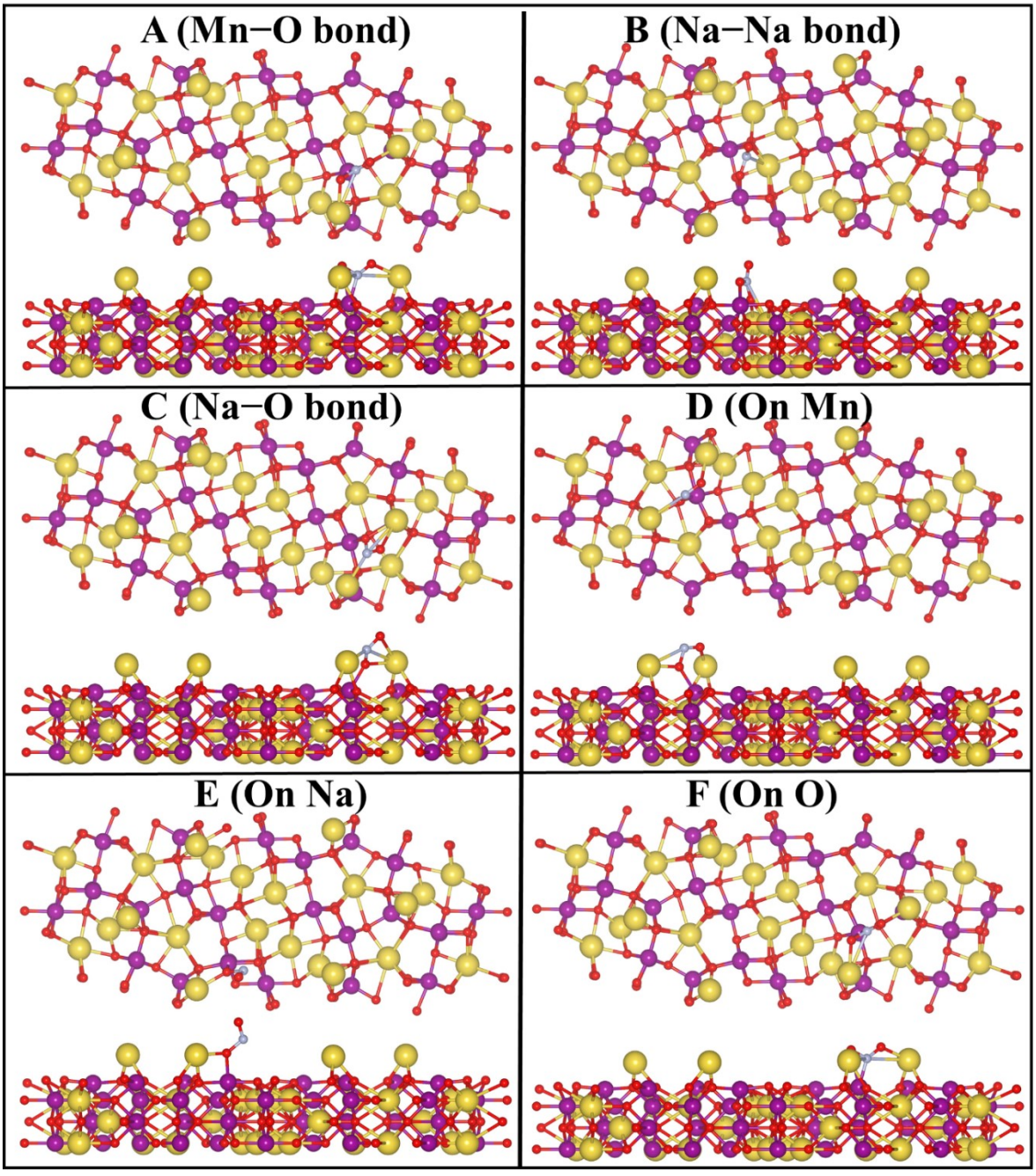

Figure S11: The stable geometries of adsorbed NO_2 gas molecules on the $Na_{0.4}MnO_2$ surface considering various site configurations. The colour codes used are as follows: Na (Yellow), Mn (Violet), and O (Red)

In the context of the interaction between NO_2 gas molecules and the $Na_{0.4}MnO_2$ surface, results confirmed that the NO_2 molecule exhibited a more significant interaction with the surface across all potential sites, except for sites **B** and **E**. During this interaction, the NO_2 molecule tends to form bonds with the Na atoms of the $Na_{0.4}MnO_2$ surface, as illustrated in **Fig. S11**. It was consistently observed that NO_2 gas molecules primarily engage with the Na and Mn atoms of the $Na_{0.4}MnO_2$ surface, regardless of their initial positions on the surface. The relative changes in the structural parameters of the NO_2 gas molecule upon interaction are compiled In **Table S4**. In the isolated form, the NO_2 molecule naturally possesses a bond angle of 133.42° and a bond length of 1.21 Å. However, upon adsorption onto the $Na_{0.4}MnO_2$ surface, the N−O bond length underwent alterations in all configurations, with a noticeable extension observed in almost all cases. Similarly, modifications in the bond angle were observed for almost all sites. Based on the adsorption energy values, it was confirmed that sites **A, C**, **D**, and **F** exhibited near-identical adsorption energies, approximately around −4.00 eV. This observation underscores the nature of the interaction between the Na and Mn atoms of the $Na_{0.4}MnO_2$ surface and the NO_2 gas molecule. The discernible alterations in bond length, bond angle, and the variations in adsorption energies across different configurations provided valuable insights into the adsorption behaviour of NO_2 on the $Na_{0.4}MnO_2$ surface.

Table S4. The altered geometrical parameters resulting from the adsorption activity of the NO_2 gas molecule on the $Na_{0.4}MnO_2$ surface, including bond length and angle, along with the corresponding adsorption energy (E_{ad}) for specific sites.

Position	E_{ad} **(eV), DFT**	E_{ad} **(eV), DFT+U**	**Bond length,** d_{N-O} **(Å)**	**Angle, ∠O−N−O (°)**
A (Mn−O)	−4.03	−3.60	1.27	118.8
B (Na−Na)	−1.95	−2.05	1.25	121.4
C (Na−O)	−3.84	−3.96	1.28	112.9
D (on Mn)	−3.86	−3.38	1.28	115.1
E (on Na)	−2.93	−2.62	1.30	111.2
F (on O)	−4.03	−3.21	1.27	118.9

In the context of the interaction between the SO_2 gas molecule and the $Na_{0.4}MnO_2$ surface, findings indicated that the SO_2 molecule demonstrated significant interaction with the surface across all potential sites, excluding the **F** site. Similar to the adsorption of the NO_2 gas molecule, the SO_2 molecule formed bonds with the Na atoms of the $Na_{0.4}MnO_2$ surface, as depicted in **Fig. S12**. A consistent trend is observed in the interaction of SO_2 gas molecules with the Na and Mn atoms of the $Na_{0.4}MnO_2$ surface, irrespective of their initial positions on the surface. The relative changes in the structural parameters of the SO_2 gas molecule upon interaction are compiled in **Table S5**. In its isolated form, the SO_2 molecule naturally possesses a bond angle of 119.37° and a bond length of 1.45 Å. However, upon adsorption onto the $Na_{0.4}MnO_2$ surface, the S−O bond length underwent alterations in all configurations, with a noticeable extension observed in almost all cases. Similarly, modifications in the bond angle are noted for almost all sites. Based on the adsorption energy values, it was confirmed that sites **A**, **B**, **D**, and **E** exhibited dominant adsorption energies, with a maximum of −3.34 eV for the D site configuration. DFT+U calculations were conducted to estimate the adsorption energy. The results indicate that persistent chemisorption behaviour is exhibited by NO_2 and SO_2 gas molecules, albeit with slight variations in their energy, potentially attributed to electron localization. Notably, a shift in the maximum adsorption energy site from an **A** site to a **C** site is demonstrated by the NO_2 gas molecule, despite observing equivalent charge transfer at both sites. Conversely, the same maximum adsorption energy site is maintained by the SO_2 gas molecule in both calculations, accompanied by a subtle increase in adsorption energy.

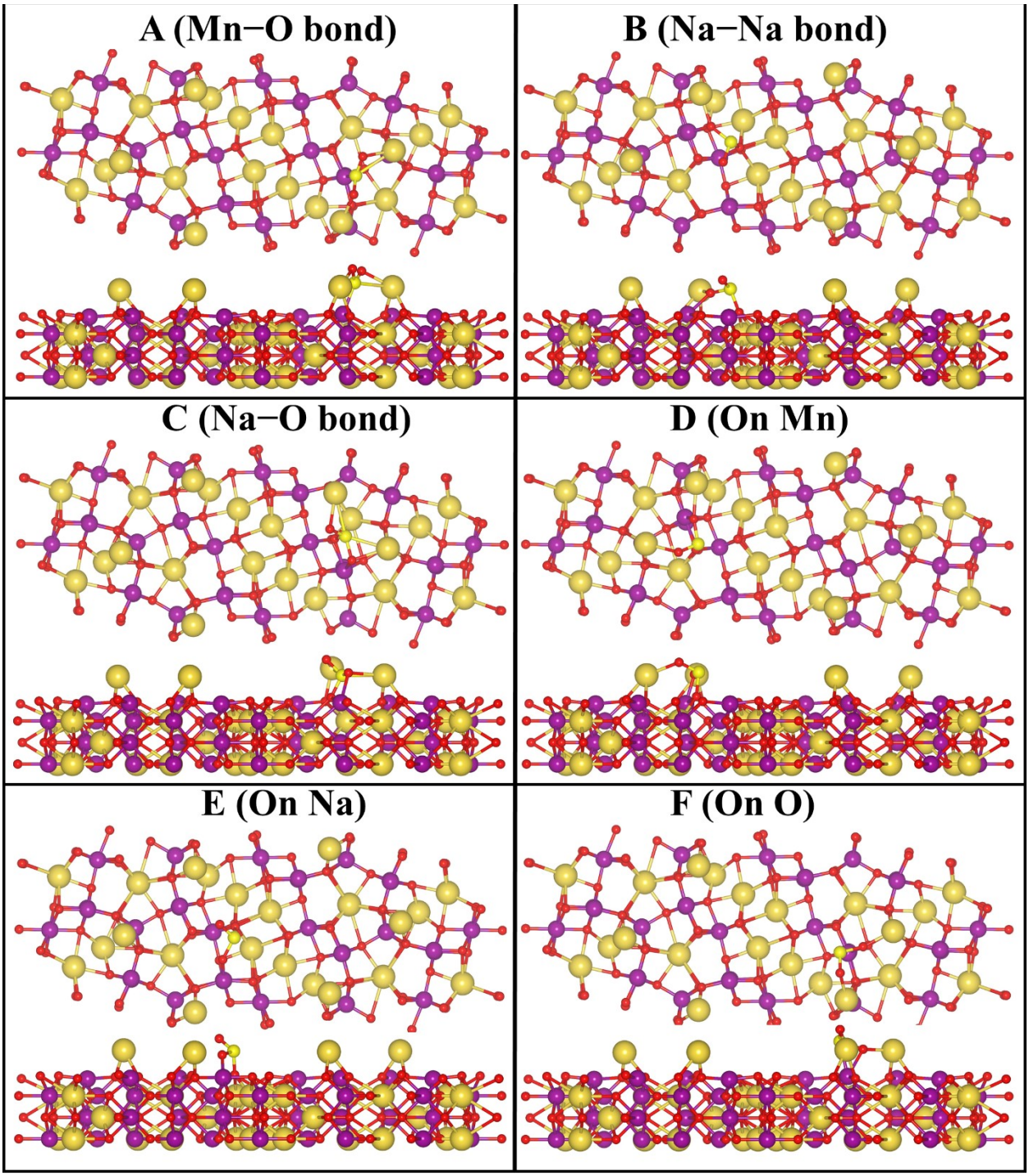

Figure S12. The stable geometries of adsorbed SO_2 gas molecules on the $Na_{0.4}MnO_2$ surface considering various site configurations. The colour codes used are as follows: Na (Yellow), Mn (Violet), and O (Red)

Table S5. The altered geometrical parameters resulting from the adsorption activity of the SO_2 gas molecule on the $Na_{0.4}MnO_2$ surface, including bond length and angle, along with the corresponding adsorption energy (E_{ad}) for specific sites.

Position	E_{ad} (eV), DFT	E_{ad} (eV), DFT+U	Bond length, $d_{N–O}$ (Å)	Angle, ∠O−N−O (°)
A (Mn−O)	−2.69	–2.62	1.50	112.0
B (Na−Na)	−2.86	–2.95	1.55	109.0
C (Na−O)	−2.36	–3.48	1.54	112.9
D (on Mn)	−3.34	–3.54	1.56	103.9
E (on Na)	−2.56	–2.94	1.54	106.9
F (on O)	−1.44	–0.43	1.55	110.6

References

1. P. Hohenberg, W. Kohn, *Phys. Rev.,* **1964**, *136*, B864.
2. W. Kohn, L.J. Sham, *Phy. Rev.,* **1965**, *140* (4A), A1133.
3. G. Kresse, J. Furthmüller, *Phys. Rev. B,* **1996**, *54* (11), 169.
4. P.E. Blöchl, *Phys. Rev. B,* **1994**, *50* (24), 17953.
5. J.P. Perdew, K. Burke, M. Ernzerhof, *Phys. Rev. Lett.,* **1996**, *77* (18), 3865.
6. H.J. Monkhorst, J.D. Pack, *Phys. Rev. B,* **1976**, *13* (12), 5188–5192.
7. S. Grimme, *J. Comput. Chem.,* **2006**, *27* (15), 1787–1799.
8. K. Momma, F. Izumi, *J. Appl. Crystallogr.* **2008**, *41* (3), 653–658.
9. G. Henkelman, A. Arnaldsson, H. Jónsson, *Comput. Mater. Sci.,* **2006**, *36* (3), 354–360.
10. S.L. Dudarev, A.B. Gianluigi, Y.S. Sergey C.J. Humphreys, and A.P. Sutton, *Phys. Rev. B*, **1998**, *57* (3), 1505.

11. M. Shishkin, S. Hirofumi, *J. Phys. Chem. C*, **2021**, *125* (2), 1531–1543.